11030 *Inorg. Chem.* **2010**, *49*, 11030–11038
DOI: 10.1021/ic101515g

Inorganic Chemistry
Article

Bis(μ-oxo) Dicopper(III) Species of the Simplest Peralkylated Diamine: Enhanced Reactivity toward Exogenous Substrates

Peng Kang,[†] Elena Bobyr,[†] John Dustman,[†] Keith O. Hodgson,*[,†,‡] Britt Hedman,*[,‡] Edward I. Solomon,*[,†,‡] and T. Daniel P. Stack*[,†]

[†]*Department of Chemistry, Stanford University, Stanford, California 94305, United States, and* [‡]*Stanford Synchrotron Radiation Lightsource, SLAC, Stanford University, Menlo Park, California 94025, United States*

Received July 28, 2010

N,N,N′,N′-tetramethylethylenediamine (TMED), the simplest and most extensively used peralkylated diamine ligand, is conspicuously absent from those known to form a bis(μ-oxo)dicopper(III) (**O**) species, $[(TMED)_2Cu(III)_2(\mu_2\text{-}O)_2]^{2+}$, upon oxygenation of its Cu(I) complex. Presented here is the characterization of this **O** species and its reactivity toward exogenous substrates. Its formation is complicated both by the instability of the $[(TMED)Cu(I)]^{1+}$ precursor and by competitive formation of a presumed mixed-valent trinuclear $[(TMED)_3Cu(III)Cu(II)_2(\mu_3\text{-}O)_2]^{3+}$ (**T**) species. Under most reaction conditions, the **T** species dominates, yet, the **O** species can be formed preferentially (>80%) upon oxygenation of acetone solutions, if the copper concentration is low (<2 mM) and $[(TMED)Cu(I)]^{1+}$ is prepared immediately before use. The experimental data of this simplest **O** species provide a benchmark by which to evaluate density functional theory (DFT) computational methods for geometry optimization and spectroscopic predictions. The enhanced thermal stability of $[(TMED)_2Cu(III)_2(\mu_2\text{-}O)_2]^{2+}$ and its limited steric demands compared to other **O** species allows more efficient oxidation of exogenous substrates, including benzyl alcohol to benzaldehyde (80% yield), highlighting the importance of ligand structure to not only enhance the oxidant stability but also maintain accessibility to the nascent metal/O_2 oxidant.

1. Introduction

Bis(μ-oxo)dicopper(III) (**O**) species have attracted considerable interests in the past decade[1−4] as a high-valent metal-oxo species that is formed by the reaction of a wide variety of Cu(I) complexes with dioxygen (O_2). Though unknown until the mid-1990s, the **O** species is now the most characterized of all Cu−O_2 products and can exist in a facile equilibrium with appreciable amounts of the isomeric, side-on μ-η^2:η^2-peroxodicopper(II) (^{S}**P**) species,[5−7] the characterized oxygenated species of tyrosinase (Tyr), catechol oxidase, and hemocyanin.[8] Given the close structural and energetic relationship of **O** and ^{S}**P** isomers, the nature of the active oxidant in tyrosinase is an open issue considering that several synthetic systems stabilizing a spectroscopically and structurally faithful ^{S}**P** mimic of oxy-Tyr are capable of hydroxylating exogenously added phenolates to catecholates through the immediacy of an **O** type species.[9]

Numerous nitrogen-based ligands have been systematically explored for their ability to stabilize **O** species,[1] such as alkyl amines,[10,11] pyridines,[12] diketiminates,[13] and most recently guanidines[14] at low temperatures (193 K) with weakly coordinating anions in non-protic solvents. The ligand attributes that correlate with **O** formation are electron-rich bidentate ligands

*To whom correspondence should be addressed. E-mail: hodgson@ssrl.slac.stanford.edu (K.O.H.), hedman@ssrl.slac.stanford.edu (B.H.), edward.solomon@stanford.edu (E.I.S.), stack@stanford.edu (T.D.P.S.).

(1) Mirica, L. M.; Ottenwaelder, X.; Stack, T. D. P. *Chem. Rev.* **2004**, *104*, 1013–1045.
(2) Lewis, E. A.; Tolman, W. B. *Chem. Rev.* **2004**, *104*, 1047–1076.
(3) Schindler, S. *Eur. J. Inorg. Chem.* **2000**, 2311–2326.
(4) Itoh, S.; Tachi, Y. *Dalton Trans.* **2006**, 4531–4538.
(5) Halfen, J. A.; Mahapatra, S.; Wilkinson, E. C.; Kaderli, S.; Young, V. G.; Que, L.; Zuberbuhler, A. D.; Tolman, W. B. *Science* **1996**, *271*, 1397–1400.
(6) Obias, H. V.; Lin, Y.; Murthy, N. N.; Pidcock, E.; Solomon, E. I.; Ralle, M.; Blackburn, N. J.; Neuhold, Y. M.; Zuberbuhler, A. D.; Karlin, K. D. *J. Am. Chem. Soc.* **1998**, *120*, 12960–12961.
(7) Mahadevan, V.; Henson, M. J.; Solomon, E. I.; Stack, T. D. P. *J. Am. Chem. Soc.* **2000**, *122*, 10249–10250.
(8) Solomon, E. I.; Sundaram, U. M.; Machonkin, T. E. *Chem. Rev.* **1996**, *96*, 2563–2605.
(9) Mirica, L. M.; Vance, M.; Rudd, D. J.; Hedman, B.; Hodgson, K. O.; Solomon, E. I.; Stack, T. D. P. *Science* **2005**, *308*, 1890–1892.
(10) Tolman, W. B. *Acc. Chem. Res.* **1997**, *30*, 227–237.
(11) Stack, T. D. P. *Dalton Trans.* **2003**, 1881–1889.
(12) Hayashi, H.; Fujinami, S.; Nagatomo, S.; Ogo, S.; Suzuki, M.; Uehara, A.; Watanabe, Y.; Kitagawa, T. *J. Am. Chem. Soc.* **2000**, *122*, 2124–2125.
(13) Spencer, D. J. E.; Aboelella, N. W.; Reynolds, A. M.; Holland, P. L.; Tolman, W. B. *J. Am. Chem. Soc.* **2002**, *124*, 2108–2109.
(14) Herres-Pawlis, S.; Verma, P.; Haase, R.; Kang, P.; Lyons, C. T.; Wasinger, E. C.; Florke, U.; Henkel, G.; Stack, T. D. P. *J. Am. Chem. Soc.* **2009**, *131*, 1154–1169.

 Published on Web 10/28/2010

Scheme 1. Peralkylated Diamine Ligands (PDLs)

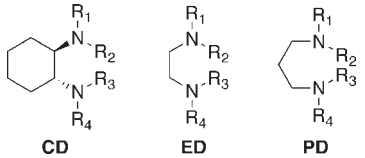

capable of stabilizing a d^8 Cu(III) center and sufficient steric demands to preclude the formation of a nonreactive $[(L)_2Cu(I)]^{1+}$ complex. Tridentate and tetradentate mononucleating, nitrogen-based ligands can stabilize the **O** species, albeit this occurs by a denticity reduction, in which ligating atoms do not associate closely with the copper centers.[1] The steric demands of the described bidentate ligands tend to stabilize three-coordinate Cu(I) complexes in which the third ligand is derived from a weakly associated anion or solvent molecule such as acetonitrile. While such complexes provide access of O_2 to the copper center and rapid formation of the **O** species, this dimer is very compact with a Cu···Cu distance of only 2.73−2.85 Å. The consequence is that neither the copper centers nor the oxide ligands are very accessible to exogenous substrates. Predictably, the larger the steric demands, the more oxidative damage that is inflicted on the ligands upon warming these **O** species to ambient conditions. Intramolecular ligand hydroxylation is a prevalent decomposition pathway,[15] thereby limiting the thermal stability of most **O** species. Directing this oxidative reactivity outward to exogenous substrates requires minimizing the steric demands of the ligands while retaining oxidatively robust substituents.

We have explored extensively the peralkylated diamine ligands (PDLs) in stabilizing **O** species as simple and versatile ligands (Scheme 1). Systematic variation of the steric demands and bite-angle provides an exquisite probe into the nature of the Cu/O_2 species formed.[11] The three most extensively explored families of PDLs, defined by their parent diamine backbone, are the (*R,R*)-1,2-cyclohexanediamines (CD),[16] 1,2-ethylenediamines (ED),[7,17] and 1,3-propanediamines (PD).[18,19] Notably in the ED series, simply reducing the steric demands of alkyl moieties, the predominant Cu/O_2 species shifts from a ^{S}**P** species[17] to an **O** species[16,20] finally to a trinuclear species, $[Cu(III)Cu(II)_2(\mu_3\text{-}O)_2]^{3+}$ (**T**),[11] demonstrating the versatility of ED ligands. The aliphatic substituents create strongly basic, tertiary N-donors, which are able to stabilize the high Cu(III) oxidation state at Cu−N distances longer than secondary amines.

N,N,N′,N′-tetramethylethylenediamine (TMED) is the most widely used PDL in Cu-catalyzed aerobic organic transformations.[21−23] CuCl/amine/O_2 combinations catalytically convert alcohols to aldehydes in high yields under ambient conditions while TMED is among the commonly employed amines. CuCl/TMED/O_2 also oxidatively couples 2,6-disubstituted phenols to form poly-2,6-disubstiuted 1,4-phenylene ethers, 2,4-disubstituted phenols to bis-phenols,[24] and acetylenes to diacetylenes in high yields.[25] However, little information is known about the active Cu/O_2 species that form with TMED and allow the reactions to be catalytic.

As the simplest PDL, TMED stands as a promising ligand to stabilize an accessible **O** species for exogenous substrates and the C−H groups of the methyl substituents should be the most oxidatively robust based on simple bond dissociation energies.[16] However, the expected **O** species with TMED is conspicuously absent from previous studies because of ambiguous and ill-defined oxygenation chemistry.[11] This study discusses the challenges and strategies to maximize the formation of the **O** species with TMED and investigates its physical properties and reactivities toward exogenous substrates.

2. Results

Synthesis of [(TMED)Cu(I)]$^{1+}$ Complex. [(TMED)Cu(I)]$^{1+}$ was synthesized by mixing equimolar amounts of TMED and [Cu(I)(MeCN)$_4$](X) ($X^- = SbF_6^-, CF_3SO_3^-$) in dry CH_2Cl_2. Slight deviations from the 1:1 Cu(I)/TMED ratio often lead to an unstable [(TMED)Cu(I)]$^{1+}$ complex or incomplete oxygenation as assessed by optical absorptions. The [(TMED)Cu(I)]$^{1+}$ solutions degrade faster compared to other PDL-Cu(I) complexes in a N_2 drybox; a yellow precipitate forms within 12 h, and over longer periods the solution turns blue accompanied with a brown precipitate presumably due to the disproportionation of the Cu(I) complex. Purification of the Cu(I) complex by a reported method[26] yields a white solid, which can be oxygenated at low temperature. However, it still turns into a yellow solid over 24 h, which no longer reacts with dioxygen at low temperatures. The ligating acetonitrile present in the white solid is lost in the yellow solid by ^{1}H NMR analysis, leading to a nonreactive Cu(I) complex toward O_2. The instability of the Cu(I) complex mandates that the Cu(I) solutions are prepared immediately before oxygenation at low temperatures for reproducible results.

Oxygenation of [(TMED)Cu(I)]$^{1+}$ Complex. [(TMED)Cu(I)](X) ($X^- = SbF_6^-, CF_3SO_3^-$) solutions were oxygenated by injection into a rapidly stirred O_2-saturated acetone solution at 183 K. The rapid full formation (< 5 s) of the **O** species is indicated by the yellow color of the initial colorless solution. The 392 nm ligand to metal charge transfer (LMCT) band (Figure 1, ε = 18.5 mM^{-1} cm^{-1} per dimer) is consistent with other related **O** species.[1] The intensity of this optical feature is not altered by purging the solution with N_2 nor by evacuating the reaction vessel, consistent with an irreversible oxygenation reaction. Titration of the **O** species with ferrocene monocarboxylic acid, a technique developed to quantify the formation of such oxidizing species,[14] gives 80% of the expected yield calibrated against well-established, fully formed **O** species (Supporting Information, Figure S1).

(15) Mahapatra, S.; Halfen, J. A.; Tolman, W. B. *J. Am. Chem. Soc.* **1996**, *118*, 11575–11586.
(16) Cole, A. P.; Mahadevan, V.; Mirica, L. M.; Ottenwaelder, X.; Stack, T. D. P. *Inorg. Chem.* **2005**, *44*, 7345–7364.
(17) Mirica, L. M.; Vance, M.; Rudd, D. J.; Hedman, B.; Hodgson, K. O.; Solomon, E. I.; Stack, T. D. P. *J. Am. Chem. Soc.* **2002**, *124*, 9332–9333.
(18) Mahadevan, V.; DuBois, J. L.; Hedman, B.; Hodgson, K. O.; Stack, T. D. P. *J. Am. Chem. Soc.* **1999**, *121*, 5583–5584.
(19) Ottenwaelder, X.; Rudd, D. J.; Corbett, M. C.; Hodgson, K. O.; Hedman, B.; Stack, T. D. P. *J. Am. Chem. Soc.* **2006**, *128*, 9268–9269.
(20) Mahadevan, V.; Hou, Z. G.; Cole, A. P.; Root, D. E.; Lal, T. K.; Solomon, E. I.; Stack, T. D. P. *J. Am. Chem. Soc.* **1997**, *119*, 11996–11997.
(21) Caulton, K. G.; Davies, G.; Holt, E. M. *Polyhedron* **1990**, *9*, 2319–2351.
(22) Mijs, W. J.; Jonge, C. R. H. I. d. *Organic Syntheses by Oxidation with Metal Compounds*; Plenum Press: New York, 1986; p 423.
(23) Paquette, L. A. *Encyclopedia of Reagents for Organic Synthesis*; John Wiley and Sons: New York, 1988; Vol. *2*, pp 1333−1336.
(24) Hay, A. S.; Blanchard, H. S.; Endres, G. F.; Eustance, J. W. *J. Am. Chem. Soc.* **1959**, *81*, 6335–6336.
(25) Hay, A. S. *J. Org. Chem.* **1962**, *27*, 3320–3321.
(26) York, J. T.; Brown, E. C.; Tolman, W. B. *Angew. Chem., Int. Ed.* **2005**, *44*, 7745–7748.

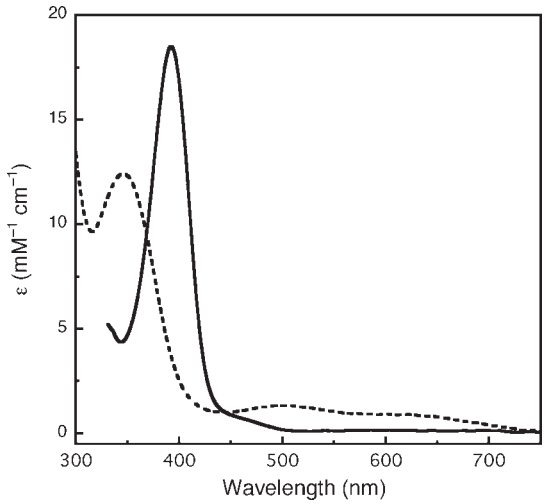

Figure 1. UV−vis spectra of the $[(TMED)_2Cu(III)_2(\mu_2\text{-}O)_2]^{2+}$ species (solid, [Cu] = 1 mM, $CF_3SO_3^-$, acetone) and proposed $[(TMED)_3Cu(III)Cu(II)_2(\mu_3\text{-}O)_2]^{3+}$ (dash, [Cu] = 1 mM, $CF_3SO_3^-$, THF) at 183 K.

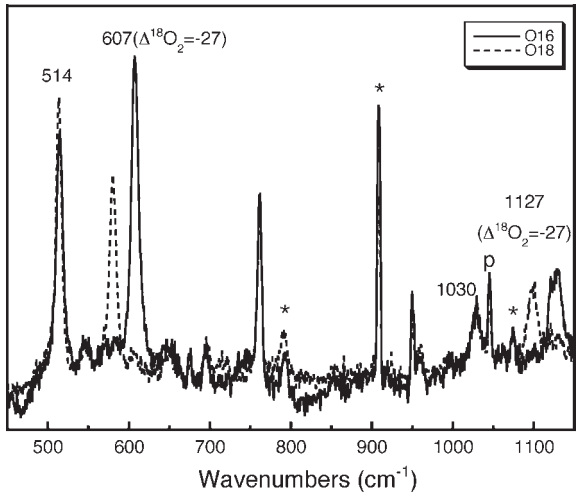

Figure 2. Resonance Raman spectra of $[(TMED)_2Cu(III)_2(\mu_2\text{-}O)_2](CF_3SO_3)_2$ species (λ_{ex} = 413.1 nm, 10% CH_2Cl_2/90% acetone, 77 K, [Cu] = 2 mM) oxygenated with $^{16}O_2$ (solid line) or $^{18}O_2$ (dash line). Solvent peaks are labeled with an * mark, and the plasma line is labeled with a "p".

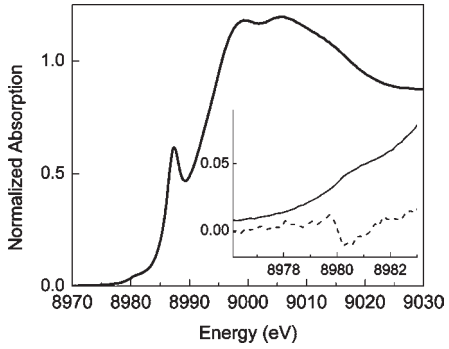

Figure 3. Normalized Cu K-edge absorption spectrum of $[(TMED)_2Cu(III)_2(\mu\text{-}O)_2](SbF_6)_2$ in acetone (5% CH_2Cl_2, [Cu] = 1 mM, 10 K). The inset shows the magnified pre-edge region (solid lines) and its smoothed second derivative (dashed lines).

This **O** species of TMED only forms in acetone at Cu concentrations less than 2 mM. At higher concentrations (>10 mM), oxygenation yields a purple solution with a dramatically different optical spectrum, presumably a 3:1 Cu/O_2 trinuclear (**T**) species (Figure 1). The most intense LMCT band of the **T** species occurs at higher energy (345 nm, ε = 12.5 mM^{-1} cm^{-1} per trimer) along with two lesser intense bands in the visible spectrum (500 nm, ε = 1.3 mM^{-1} cm^{-1}; 620 nm, ε = 0.9 mM^{-1} cm^{-1} per trimer). The energies and extinction coefficients of these three optical features are similar to other reported **T** species with *N,N′*-diethyl-*N,N′*-dimethylethylenediamine (MEED),[11] *N,N,N′,N′*-(*R,R*)-1,2-cyclohexanediamine (TMCD),[27] and *N,N*-dimethyl-2-(2-pyridyl)-ethylamine ($^{H}Py1^{Me,Me}$).[28] Once the **T** species or the **O** species is formed, no measurable equilibrium between the two species could be detected optically by varying the temperature (183−233 K) or by removing excess O_2.

Resonance Raman Spectroscopy. The resonance Raman spectrum was obtained by excitation into the 392 nm LMCT band at 413 nm (Figure 2). The characteristic symmetric Cu_2O_2 bis-μ-oxo breathing mode of the **O** species occurs at 607 cm^{-1}, shifting by 27 cm^{-1} to 580 cm^{-1} upon $^{18}O_2$ substitution.[29] The peak at 514 cm^{-1} is presumably a Cu−N stretching mode, which is not sensitive to $^{18}O_2$ isotope substitution. The feature at 1127 cm^{-1}, which shifts by 27 cm^{-1} with $^{18}O_2$ substitution, is consistent with a combination mode of the symmetric core breathing mode at 607 cm^{-1} and the Cu−N stretching mode at 514 cm^{-1}. The peak at 1030 cm^{-1} is presumably an overtone of the Cu−N stretching mode at 514 cm^{-1}, and the peaks at 762 and 950 cm^{-1} are unassigned ligand stretching modes.

X-ray Absorption Spectroscopy. Cu K-edge X-ray absorption spectroscopy (XAS) was used to probe the oxidation state of the copper centers and structural parameters of the **O** species. The XAS data with a SbF_6^- anion in acetone (5% CH_2Cl_2, 1 mM Cu) are most consistent with an **O** species. The X-ray absorption edge displays a 1s → 3d pre-edge feature at 8980.3 ± 0.2 eV (Figure 3). This value is close to the range of pre-edge values of previously characterized Cu(III) complexes (8981.0 ± 0.5 eV) and is higher than the pre-edge energy for Cu(II) complexes (8979.0 ± 0.5 eV).[30] Similarly, the pre-edge peak of a closely related **O** complex, $[(TMPD)_2Cu(III)_2(\mu_2\text{-}O)_2]^{2+}$ (TMPD = *N,N,N′N′*-tetramethyl-1,3-propanediamine), occurs at 8980.5 eV, an energy value at the lower end of the range expected for a Cu(III) species.[18] The edge exhibits an intense absorption at 8987.3 eV (Figure 3) that is assigned as a 1s → 4p + shakedown transition for Cu(II) and Cu(III) complexes and is significantly more pronounced for Cu(III) than for Cu(II).[30] The EXAFS data are fitted adequately with a model consisting of 2 O at 1.80 Å (σ^2 = 0.0038 Å^2), 2 N at 1.96 Å (σ^2 = 0.0041 Å^2), 1 Cu at 2.74 Å (σ^2 = 0.0026 Å^2), and 6 C at 2.77 Å (σ^2 = 0.0207 Å^2) (Figure 4). The short Cu−O and Cu−Cu distances are characteristic of an **O** core, which

(27) Cole, A. P.; Root, D. E.; Mukherjee, P.; Solomon, E. I.; Stack, T. D. P. *Science* **1996**, *273*, 1848–1850.
(28) Taki, M.; Teramae, S.; Nagatomo, S.; Tachi, Y.; Kitagawa, T.; Itoh, S.; Fukuzumi, S. *J. Am. Chem. Soc.* **2002**, *124*, 6367–6377.
(29) (a) Henson, M. J.; Mukherjee, P.; Root, D. E.; Stack, T. D. P.; Solomon, E. I. *J. Am. Chem. Soc.* **1999**, *121*, 10332–10345. (b) Holland, P. L.; Cramer, C. J.; Wilkinson, E. C.; Mahapatra, S.; Rodgers, K. R.; Itoh, S.; Taki, M.; Fukuzumi, S.; Que, L.; Tolman, W. B. *J. Am. Chem. Soc.* **2000**, *122*, 792–802.
(30) DuBois, J. L.; Mukherjee, P.; Stack, T. D. P.; Hedman, B.; Solomon, E. I.; Hodgson, K. O. *J. Am. Chem. Soc.* **2000**, *122*, 5775–5787.

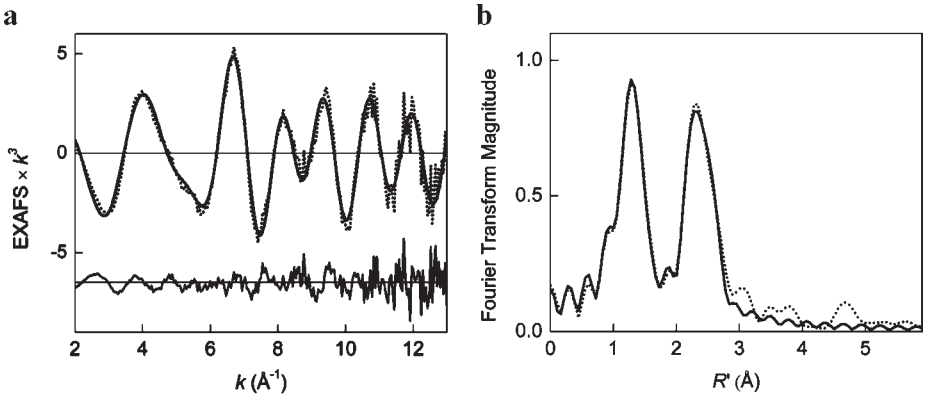

Figure 4. (a) Cu K-edge k^3-weighted EXAFS data for $[(TMED)_2Cu(III)_2(\mu_2\text{-}O)_2](SbF_6)_2$ (top) with offset fit residual (bottom) and (b) corresponding nonphase shift corrected Fourier transforms. Data (dotted lines); fit (solid lines).

typically exhibit a Cu−O bond length of 1.79−1.86 Å and a Cu···Cu separation of 2.74−2.91 Å.[1] Identical structural parameters were obtained for the **O** species with the $CF_3SO_3^-$ and SbF_6^- counteranions (Supporting Information, Figure S2 and Table S1), suggesting that neither anion closely associates with the Cu_2O_2 core.

Thermal Decomposition. Thermal decomposition kinetics and products were examined to elucidate the decomposition mechanism of this **O** species. The decay of the **O** species, initially formed in acetone at 183 K and rapidly warmed to an appropriate temperature, was monitored by the disappearance of the 392 nm UV−vis feature. The decay was recorded at various temperatures (256−279 K), and the time-dependent spectra (320−600 nm) at each temperature were fitted by a multiwavelength analysis as a simple first order A→B process. An Eyring analysis (Supporting Information, Figure S3) gave a $\Delta H^{\ddagger} = 15(1)$ kcal mol^{-1} and $\Delta S^{\ddagger} = -15(2)$ cal K^{-1} mol^{-1}. The ligand products recovered after a basic workup were ca. 75% intact ligand and 25% monodemethylated ligand as assessed by GC and GC-MS analysis, accounting for a 50% yield in ligand N-dealkylation. This analysis assumes the **O** species as a 2-electron oxidant.

Reactivity with Exogenous Substrates. $[(TMED)_2Cu(III)_2(\mu_2\text{-}O)_2]^{2+}$ stoichiometrically oxidizes benzyl alcohol and phenolic substrates at 243 K. Two equivalents of alcohol or phenol substrates were added to the **O** species after the removal of excess O_2 by multiple cycles of purging and evacuation, and the decay kinetics of the **O** species were monitored at 392 nm until this optical feature was fully quenched each time. After an aqueous workup, the organic products were quantified by GC and/or GC-MS for alcohol substrates and by ^{1}H NMR for the phenolic substrates. Assuming that the **O** species serves as a 2-electron oxidant, benzyl alcohol is oxidized to benzaldehyde in a ca. 80% yield, whereas octanol does not react. 2,4-Di-*tert*-butylphenol is coupled to 3,3′,5,5′-tetra-*tert*-butyl-2,2′-bisphenol in a ca. 40% yield, consistent with ca. 50% maximum yield measured from other **O** species with excess O_2 fully removed.[14,31]

The mechanism of benzyl alcohol oxidation was further probed using various deuterated benzyl alcohols both by competitive and absolute measurements of the rate of decay of $[(TMED)_2Cu(III)_2(\mu_2\text{-}O)_2]^{2+}$ species. The intramolecular competition experiment of the oxidation of α-d_1-benzyl alcohol gave a 2.8(1):1 α-d_1-benzaldyhyde/α-h_1-benzaldyhyde ratio by GC-MS analysis, indicating clearly that αC−H(D) bond cleavage occurs in the product determining step of the reaction (Table 1). The intermolecular competition experiments with a 1:1 mixture of α,α-h_2 and α,α-d_2 benzyl alcohol are consistent with the intramolecular results, yielding a 3.5(2):1 ratio of α-h_1-benzaldyhyde/α-d_1-benzaldyhyde.[32] The absolute rate of the oxidation of α,α-h_2 and α,α-d_2 benzyl alcohol were measured independently at 243 K by monitoring the decay of the 392 nm **O** feature using a 20-fold excess of substrate. Under these conditions, a pseudo first-order decay was measured for each substrate yielding a KIE value (k_h/k_d) of 3.3(4). The comparable competitive and absolute kinetic isotope effects are consistent with a single rate and product determining step involving C−H bond cleavage. Deuteration of the hydroxyl proton on benzyl alcohol marginally impacted the oxidation rate (KIE = 1.12(7), Table 1).

Table 1. Kinetic Isotope Effects in the Oxidation of Deuterated Benzyl Alcohols

substrates	$PhCH_2OH$/$PhCD_2OH$ [a]	PhCHD-OH [b]	$PhCH_2OH$ + $PhCD_2OH$ [c]	$PhCH_2OH$/$PhCH_2OD$ [a]
KIE	3.3(4)	2.8(1)	3.5(2)	1.12(7)

[a] k_H/k_D from independent kinetic measurements by UV−vis (20 equiv of alcohol, averaged from three measurements). [b] The PhCDO/PhCHO ratio in the reaction product. [c] The PhCHO/PhCDO ratio in the reaction product.

DFT Computations. The geometry of $[(TMED)_2Cu(III)_2(\mu_2\text{-}O)_2]^{2+}$, optimized by density functional theory (DFT) calculations, is significantly more stable than that of the ^{S}**P** isomer (vacuum, electronic energies: 7.8 kcal mol^{-1} at B3LYP/BS1//B3LYP/6-31G(d),[33] 15.1 kcal mol^{-1} at BLYP/BS1//B3LYP/6-31G(d)). The optimized metrical parameters of the **O** species are variable depending upon the functional and basis set used (Table 2). In all cases, no core potentials were used for the copper centers, as such basis sets expand the $Cu_2O_2N_4$ cores relative to experimental metrical values. An increase in the Hartree−Fock (HF)

(31) (a) Osako, T.; Ohkubo, K.; Taki, M.; Tachi, Y.; Fukuzumi, S.; Itoh, S. *J. Am. Chem. Soc.* **2003**, *125*, 11027–11033. (b) Pavlova, S. V.; Chen, K. H. C.; Chan, S. I. *Dalton Trans.* **2004**, 3261–3272.

(32) Pratt, R. C.; Stack, T. D. P. *Inorg. Chem.* **2005**, *44*, 2367–2375.

(33) The hybrid functional B3LYP tends to over-stabilize the ^{S}**P** isomer compared to the pure functional BLYP. See: Lewin, J. L.; Heppner, D. E.; Cramer, C. J. *J. Biol. Inorg. Chem.* **2007**, *12*, 1221–1234.

Table 2. Metrical Parameters Optimized by Different DFT Methods for $[(TMED)_2Cu(III)_2(\mu_2\text{-}O)_2]^{2+}$

functional/basis set	Cu···Cu (Å)	O···O (Å)	Cu−O (Å)	Cu−N (Å)
BLYP/6-31G(d)	2.77	2.33	1.81	1.97
B3LYP/6-31G(d)	2.72	2.31	1.79	1.95
BHandHLYP/6-31G (d)	2.66	2.30	1.76	1.94
BLYP/BS1[a]	2.82	2.37	1.84	2.02
B3LYP/BS1[a]	2.76	2.34	1.81	1.99
BHandHLYP/BS1[a]	2.69	2.32	1.77	1.96
experiment (EXAFS)	2.74		1.80	1.96

[a] BS1 uses a 6-311+G(d) basis set on Cu, O, and N atoms and a 6-31G(d) basis set on C and H atoms.

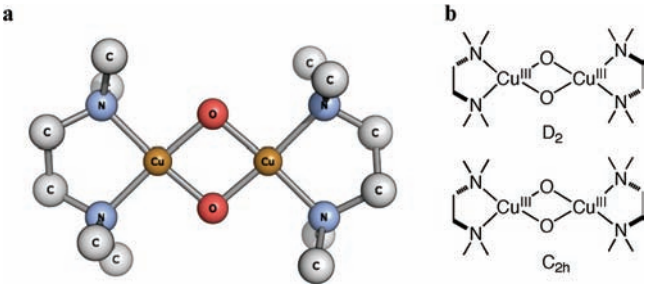

Figure 5. (a) DFT optimized D_2 geometry of $[(TMED)_2Cu(III)_2(\mu_2\text{-}O)_2]^{2+}$ with B3LYP/6-31G(d) method (hydrogen atoms are omitted for clarity): Cu−O = 1.79 Å, Cu−N = 1.95 Å, Cu···Cu = 2.72 Å, O···O = 2.31 Å. (b) Scheme of two limiting high-symmetry conformations.

percentage in the functional (from 0% in BLYP to 50% in BHandHLYP) or a reduction in the size of basis set (from BS1 to 6-31G(d)) generally leads to shorter Cu···Cu and Cu−O distances. The B3LYP/6-31G(d) optimized structure (Figure 5a) provides the closest agreement with the metrical parameters from the experimental-derived EXAFS model. The two limiting, high-symmetry conformations (D_2 and C_{2h}, Figure 5b) exist for $[(TMED)_2Cu(III)_2(\mu_2\text{-}O)_2]^{2+}$ resulting from the relative twisting of the 5-membered chelate rings of the ligands. The optimized D_2 structure is ca. 0.3 kcal mol^{-1} lower in energy with the energy evaluated at a B3LYP/BS1 level of theory (B3LYP/BS1//B3LYP/6-31G(d)). All subsequent computations used this D_2 optimized geometry. The non-scaled[34] computed Raman spectrum predicts an intense A_1 Cu_2O_2 breathing mode at 679 cm^{-1} that shifts to 647 cm^{-1} (Δ = 32 cm^{-1}) upon $^{18}O_2$ substitution (Table 3). This compares favorably with the 607 cm^{-1} experimental resonance Raman feature of the Cu_2O_2 core mode (λ_{ex} = 413 nm) that shifts to 580 cm^{-1} (Δ = 27 cm^{-1}) upon $^{18}O_2$ substitution. The vibration calculation also predicts an intense A_1 symmetric Cu_2O_2 vibration mode at 141 cm^{-1} that is ^{18}O isotope insensitive in agreement with experimental values for other simple **O** species formed with PDLs (ca. 120−135 cm^{-1}).[29]

Theoretical electronic spectra were calculated using time-dependent DFT (TD-DFT) with various methods (Table 4). Increasing the percentage of HF in the functional or reducing the basis set size results in a blue-shift of the ca. 390 nm LMCT band. While a PCM solvation model only marginally shifts the energy of this feature, the relative oscillator strengths of the 390 nm band with

Table 3. Selected Experimental Resonance Raman and Calculated Raman Vibration Modes (B3LYP/6-31G(d)) for $[(TMED)_2Cu(III)_2(\mu_2\text{-}O)_2]^{2+}$

normal mode (^{18}O isotope downshift)	experimental (cm^{-1})	DFT (cm^{-1})
Cu_2O_2 breathing	607 (27)	679 (32)
Cu−N	514 (0)	541 (1)
Cu_2O_2 flexing		141 (0)

Table 4. Experimental and Calculated Absorption Spectra (TD-DFT) on the D_2 Symmetric Geometry $[(TMED)_2Cu(III)_2(\mu_2\text{-}O)_2]^{2+}$ Optimized at B3LYP/6-31G(d) Level

functional/basis set	wavelength (nm)	oscillator strength	wavelength (nm)	oscillator strength
experiment	392	0.23		
	Vacuum			
BLYP/6-31G(d)	375	0.12	301	0.63
B3LYP/6-31G(d)	338	0.28	274	0.63
BHandHLYP/6-31G(d)	298	0.54	234	0.56
BLYP/BS1	393	0.11	311	0.72
B3LYP/BS1	354	0.25	286	0.65
BHandHLYP/BS1	311	0.54	245	0.55
	PCM[a]			
BLYP/6-31G(d)	376	0.16	305	0.67
B3LYP/6-31G(d)	340	0.36	276	0.67
BHandHLYP/6-31G(d)	301	0.66	235	0.59
BLYP/BS1	393	0.15	315	0.80
B3LYP/BS1	357	0.34	289	0.69
BHandHLYP/BS1	315	0.66	246	0.57

[a] Acetone (dielectric ε = 20.7) with United Atom Topological Model (UA0) radii.

another predicted about 290 nm LMCT band are much more balanced, consistent with other **O** species investigated in solvents that allow both bands to be measured.[1] A simulated spectrum using the experimental bandwidth of the 392 nm feature (Figure 6) shows a LMCT at 357 nm (ε = 30 mM^{-1} cm^{-1}) compared to the 392 nm (ε_{corr} = 23 mM^{-1} cm^{-1})[35] experimental value. Population analysis (Supporting Information, Table S2) suggests that this LMCT band is composed partially of a dioxo σ^* orbital (HOMO-1) to Cu d_{xy} orbital (LUMO+1) transition, consistent with previous assignments in the literature.[29] Another intense LMCT band is predicted at ca. 290 nm; population analysis supports a dioxo π_σ^* orbital (HOMO-5) to Cu d_{xy} orbital (LUMO) transition. This feature is not observed experimentally because of the acetone solvent absorption in this region.

3. Discussion

Formation of the O Species. A diverse array of thermally sensitive species are formed in the reaction of Cu(I) complexes with O_2. The formation and stabilization of such species depends on ligand, concentration of copper, solvent, counteranion, and temperature.[1] With Cu(I) complexes that react with O_2, the steric demands of the ligand predominately determine the type of Cu/O_2 species that forms with the ligand electronics, solvent, counteranions, and temperature playing an important but subordinate role. In the present study, the limited ligand steric demands of *N,N,N′,N′*-tetramethylethylenediamine

(34) The scale factor for the frequency calculation at B3LYP/6-31G(d) is 0.952. See: Alecu, I. M.; Zheng, J.; Zhao, Y.; Truhlar, D. G. *J. Chem. Theory Comput.* **2010**, *6*, 2872–2887.

(35) The extinction coefficient is corrected from the experimental value assuming an 80% formation of TMED **O** species estimated from a FcCOOH titration.

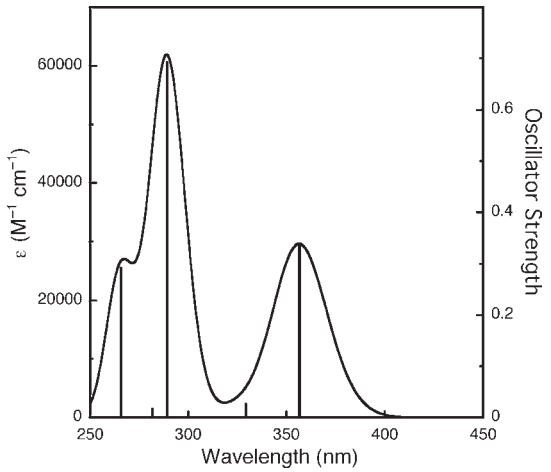

Figure 6. Oscillator strength and simulated electronic spectra of $[(TMED)_2Cu(III)_2(\mu_2\text{-}O)_2]^{2+}$ from DFT calculation with PCM-TD-B3LYP/BS1//B3LYP/6-31G(d) method (FWHM = 2500 cm^{-1}).

(TMED) in $[(TMED)Cu(I)]^{1+}$ very much complicates its oxygenation reaction as two spectroscopically distinct, thermally sensitive $Cu-O_2$ species are formed with a 2:1 and 3:1 Cu/O_2 stoichiometry. The former is characterized in this study as the $[(TMED)_2Cu(III)_2(\mu_2\text{-}O)_2]^{2+}$ complex, an **O** species, and the latter is postulated as a trinuclear $[(TMED)_3Cu(III)Cu(II)_2(\mu_3\text{-}O)_2]^{3+}$ complex, a **T** species. Additional complications in the oxygenation reaction result from the limited stability of $[(TMED)Cu(I)]^{1+}$ with weakly coordinating anions in aprotic, dry solvents, even under an inert atmosphere. Peralkylated diamine (PDL) Cu(I) complexes generally ligate one or two acetonitrile ligands, creating either a trigonal or a tetrahedral complex, respectively. Acetonitrile loss and anion association to the copper center often leads to degradation or oligomerization of the complexes, which is prominent with less sterically demanding PDLs such as TMED with an exposed copper center. In this case, the resulting yellow precipitate does not oxygenate to a detectable, thermal-sensitive species under our standard conditions. Degradation of a rapidly precipitated white solid of $[(TMED)Cu(I)]^{1+}$ even occurs in the solid state under a dinitrogen atmosphere at room temperature. The least sterically demanding ligands such as TMED can also form a colorless 2:1 complex, $[(TMED)_2Cu(I)]^{1+}$, that has been structurally characterized[36] and does not oxygenate readily.

These complications clearly explain the dearth of data on the oxygenated forms of $[(TMED)Cu(I)]^{1+}$, especially considering that the perethylated variant, *N,N,N′,N′*-tetraethylethylenediamine (TEED), forms an isolable Cu(I) complex that oxygenates cleanly to an **O** species. Yet, the simplicity of TMED warrants an investigation if only to determine the reactivity of the **O** species in its most sterically unencumbered form. The conditions that best stabilize in situ prepared $[(TMED)Cu(I)]^{1+}$ use weakly coordinating anions such as SbF_6^- and $CF_3SO_3^-$ in dry CH_2Cl_2. Much faster degradation occurs with the more coordinating $CH_3SO_3^-$ anion in dry CH_2Cl_2. Even given the optimized conditions for stabilizing $[(TMED)Cu(I)]^{1+}$, the most reproducible oxygenation results were collected from freshly prepared solutions and then only with an 80% yield, as assessed by a titration with FcCOOH.

Scheme 2. Proposed Mechanism for Formation of **O** and **T** Species (L = Ligand)

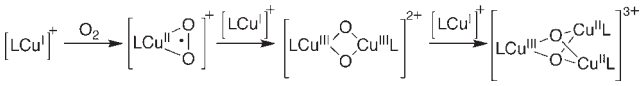

A second challenge in maximizing the formation of the **O** species is the competitive formation of a presumed **T** species. The **T** species is known to form preferentially with ligands possessing limited steric demands. Ostensibly minor changes, such as the substitution of one ethyl for one methyl substituent in a PDL, is sufficient to change from predominant **O** to predominant **T** formation at parity of other conditions. High initial copper concentrations (> 10 mM) are also known to favor the formation of **T** species.[27] The preferential formation of a **T** species are consistent with a pathway that involves a 2:1 Cu/O_2 species (an **O** or isomeric side-on peroxo species) as detailed in Scheme 2. The limited steric demands of the ligand are needed to accommodate the compact trinuclear $[Cu_3(\mu_3\text{-}O)_2]^{3+}$ core, and the high concentrations of Cu(I) are needed to rapidly trap the 2:1 species rather than allowing complete formation of the **O** species. Trimerization can be suppressed by ligands with greater steric demands allowing exclusive formation of **O** species. The facile formation of the **T** species with $[(TMED)Cu(I)]^{1+}$ suggests a susceptible Cu_2O_2 core that motivates trapping this **O** species and exploring its reactivity with other exogenous substrates.

Despite the dominance of the **T** species with TMED under most circumstances, the **O** species can be stabilized kinetically. By optimizing experimental conditions, the **O** species is made observable only in acetone combined with low initial concentrations of Cu (≤2 mM). The concentration dependent oxygenation is similar to that of small PDLs such as TMCD[27] and MEED,[11] which yield **O** species at low Cu concentrations and **T** species at high concentrations. At high Cu(I) concentrations (> 10 mM), $[(L)Cu(I)]^{1+}$ is in excess of the dissolved O_2 allowing for the bimolecular reaction of $[(L)Cu(I)]^{1+}$ with an **O** species to form a **T** species to be competitive with the initial oxygenation reaction. At low Cu(I) concentrations relative to dissolved O_2, the oxygenation reaction to form an **O** species is much faster allowing its complete formation as the kinetic product. Critical to this analysis is the fact that the dissociation reaction of O_2 from an **O** species is effectively non-existent. Acetone has a high O_2 solubility[37] relative to CH_2Cl_2 and THF thereby favoring the formation of **O** species at parity of Cu(I) concentration.

Spectral Properties. The nature of the **O** species with TMED is confirmed by UV−vis spectroscopy, resonance Raman, and XAS studies. In the UV−vis spectra, the 392 nm band with a corrected extinction coefficient of 23 mM^{-1} cm^{-1} per dimer[35] is characteristic of an **O** species. The band is blue-shifted compared to other PDL **O** species, the

(36) Pasquali, M.; Floriani, C.; Venturi, G.; Gaetanimanfredotti, A.; Chiesivilla, A. *J. Am. Chem. Soc.* **1982**, *104*, 4092–4099.

(37) Battino, R. *IUPAC Solubility Data Series, Oxygen and Ozone*, 1st ed.; Pergamon: Oxford; New York, 1981; Vol. 7.

Scheme 3. Proposed N-Dealkylation Decomposition Mechanism of $[(TMED)_2Cu(III)_2(\mu_2\text{-}O)_2]^{2+}$ Species

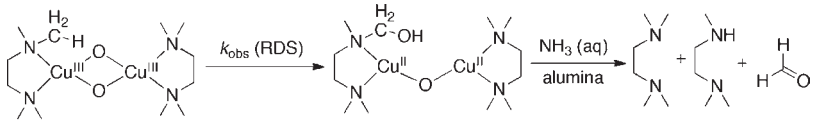

features of which are typically observed between 398 to 450 nm.[1] The 607 cm^{-1} band in resonance Raman spectra, shifted 27 cm^{-1} upon $^{18}O_2$ substitution, is attributed to the breathing mode of the Cu_2O_2 core.[29] The unusually intense Cu−N stretching mode at 514 cm^{-1} and the combination of the Cu_2O_2 breathing mode and Cu−N mode at 1127 cm^{-1} indicates that the excitation into the oxo to Cu(III) CT transition results in significant Cu−N distortions. The 1s → 3d transition of Cu in the pre-edge of XAS spectra is located at 8980.3 eV, consistent with the Cu(III) oxidation state.[30] The short Cu···Cu and Cu−O distances obtained from the EXAFS fit also agree with the characteristics of a typical **O** species.

Thermal Stability. At a given temperature, the **O** species with TMED is thermally more stable than almost all other **O** species created with PDLs. The decomposition rate (4.8×10^{-4} s^{-1}) is more than 10-fold slower than that measured for the perethylated ligand TEED (7.0×10^{-3} s^{-1}) under identical experimental conditions (263 K, acetone, [Cu] = 1 mM, $CF_3SO_3^-$). The improved thermal stability is consistent with the higher activation enthalpy and entropy derived from Eyring analyses[16] (TMED: $\Delta H^{\ddagger} = 15(1)$ kcal mol^{-1}, $\Delta S^{\ddagger} = -15(2)$ cal K^{-1} mol^{-1}; TEED: $\Delta H^{\ddagger} = 14(1)$ kcal mol^{-1}, $\Delta S^{\ddagger} = -13(1)$ cal K^{-1} mol^{-1}). Further analysis of the thermal decomposition products reveals 25% of the ligand is demethylated to form *N,N,N′*-trimethylethylenediamine, which suggests that TMED undergoes $N-CH_3$ hydroxylation at a 50% yield, assuming a $2e^-$ oxidation by the **O** species.

Ligand hydroxylation is observed frequently in the thermal decomposition of **O** species,[2,15,16,38] during which a C−H bond of the ligand is oxygenated by the Cu_2O_2 core (Scheme 3). This reaction is assumed generally to proceed through a hydrogen atom abstraction mechanism as the proton and electron derive from the same C−H bond. From previous deuterium KIE studies,[15,16] the C−H cleavage is the rate limiting step and therefore variations in the C−H bond dissociation energy (BDE) will differentiate the thermostability of the **O** species when the rest of ligand properties remains the same. The C−H BDE of a methyl group of TMED is estimated ∼2 kcal mol^{-1} higher than that of the ethyl group of TEED.[39] Given the same ethylenediamine backbone, the TMED **O** species should be the thermally most stable **O** species in the ED series.

Reactivity with Exogenous Substrates. 2,4-Di-*tert*-butylphenol and benzyl alcohol are chosen as representative substrates for reactivity studies of the **O** species. The phenol is coupled to the bis-phenol by many **O** species, including ones with very sterically demanding diamines. The generality of this reaction is consistent with a stepwise ET-PT mechanism as proposed by Itoh et al.[31] The small reported KIE (1.21−1.56) associated with O−H(D) cleavage of phenol by an **O** species is a lower bound of known PCETs, leading to the postulate that the single electron transfer from the phenol may be the first and rate-limiting step. As an ET can occur by an outer-sphere mechanism, the phenolic substrate does not need to directly access the **O** core. Therefore most **O** species, including both sterically crowded and uncrowded ones, should be capable of phenol oxidation.

The limited steric demands of the TMED ligand open the possibility of direct substrate access to the Cu_2O_2 core and an inner-sphere oxidation pathway. The TMED **O** species oxidizes benzyl alcohol to benzaldehyde efficiently (80% yield) at low temperatures without the aid of any deprotonation reagent, which is not observed with any other **O** species formed with PDLs.[40] Isotope studies provide valuable insights into the mechanism. The KIE (O−H/O−D) value of ca. 1 suggests that the cleavage of the O−H bond is not involved in the rate limiting step. The KIE values of ca. 3, determined both from independent absolute rate kinetic measurements and from intra- and intermolecular competitive reactions, suggest that the C−H bond cleavage is both the rate and product determining step. The KIE in this study is comparable to those reported for hydrogen atom transfer reaction on substrates with benzylic and aliphatic C−H bonds by high-valent metal-oxo species.[41−43] If the benzyl alcohol oxidation by the **O** species follows a similar mechanism, an exposed **O** core is critical to allow the formation of an O···H···C transition state.

4. Conclusion

The current study presents an experimental and theoretical investigation of the simplest of the bis(μ-oxo)dicopper(III) (**O**) species stabilized by the TMED ligand, with the intention of assessing the oxidizing ability of an accessible **O** core to exogenous substrates. Unlike most other PDLs, the oxygenation chemistry of the cuprous complex of TMED is complicated as a dimeric **O** species or a trimeric **T** species can be formed. A low concentration of $[(TMED)Cu(I)]^{1+}$ relative to the O_2 concentration in acetone with weakly coordinating counter-anions leads to preferential formation of the **O** species, the kinetic product. This dimeric species has been spectroscopically characterized by UV−vis, resonance Raman, and XAS, and these spectral and metrical features correlate closely with DFT calculations. The enhanced thermal stability of this species presumably results from the higher C−H bond dissociation energy of methyl groups, thereby slowing

(38) Itoh, S.; Taki, M.; Nakao, H.; Holland, P. L.; Tolman, W. B.; Que, L.; Fukuzumi, S. *Angew. Chem., Int. Ed.* **2000**, *39*, 398–400.
(39) Wayner, D. D. M.; Clark, K. B.; Rauk, A.; Yu, D.; Armstrong, D. A. *J. Am. Chem. Soc.* **1997**, *119*, 8925–8932.
(40) **O** species of *N,N,N′,N′*-tetramethyl-1,3-propanediamine (TMPD) reported by Stack, T. D. P.; et al. *J. Am. Chem. Soc.* **1999**, *121*, 5583 can oxidize benzyl alcohol to benzaldehyde in the presence of triethylamine; however, no significant KIE of O-H(D) or C-H(D) is observed, suggesting a different oxidation mechanism from the TMED **O** species.
(41) Mayer, J. M. *Acc. Chem. Res.* **1998**, *31*, 441–450.
(42) Gardner, K. A.; Mayer, J. M. *Science* **1995**, *269*, 1849–1851.
(43) Bell, S. R.; Groves, J. T. *J. Am. Chem. Soc.* **2009**, *131*, 9640–9641.

the intramolecular ligand hydroxylation as a decomposition pathway. The more exposed and accessible core of this **O** species correlates with an enhanced oxidative capacity as it cleanly oxidizes benzyl alcohol, which has not been observed previously for such Cu/O_2 species.

5. Experimental Section

Materials and Methods. All the chemicals were purchased from commercial sources if not mentioned otherwise. CH_2Cl_2, THF, and MeCN were of HPLC grade and further purified by a Pure-Solv 400 solvent purification system (Innovative Technology), HPLC grade acetone was distilled under a N_2 atmosphere after refluxing for 5 h over K_2CO_3. $[Cu(MeCN)_4]X$ ($X^- = CF_3SO_3^-$ or SbF_6^-) was synthesized from Cu_2O (Aldrich) and trifluoromethanesulfonate acid (Aldrich) or hexafluoroantimonic acid (Aldrich) by a variation of the literature method.[44] *N,N,N′,N′*-tetramethylethylenediamine (TMED) was purchased from Aldrich and distilled from CaH_2 under a N_2 atmosphere. Ferrocene monocarboxylic acid (FcCOOH) (Aldrich, 97%) was purified by sublimation in vacuum. Preparation and manipulation of air-sensitive materials were carried out in a N_2 drybox (M. Braun, 1 ppm in O_2 and H_2O). Low-temperature UV−vis spectra were collected on a Varian Cary 50 Bio spectrophotometer with a custom-designed quartz fiber-optic dip-probe (Hellma) of variable optical path length (0.10 or 1.0 cm) in custom-designed sample cells (ChemGlass).

Synthesis and Oxygenation of $[(TMED)Cu(I)]^{1+}$ Complex. Under an inert atmosphere, equimolar amounts (0.100 mmol) of $[Cu(MeCN)_4](CF_3SO_3)$ and TMED were mixed in 5 mL of CH_2Cl_2 to yield a clear, colorless solution. This solution was used immediately after preparation. In a typical oxygenation reaction, 250 μL of freshly prepared Cu(I) solution was injected into 5 mL of acetone saturated with O_2 (1 atm) under vigorous stirring at 183 K, yielding a solution of ca 0.5 mM $[(TMED)_2Cu(III)_2(\mu_2\text{-}O)_2]^{2+}$. If oxygenation occurs at higher copper concentrations ([Cu] > 10 mM), the $[(TMED)Cu(I)]^{1+}$ solution was first injected into chilled acetone under N_2 followed by purging the head space of the reaction vessel with O_2, yielding a solution of dominantly $[(TMED)_3Cu(III)Cu(II)_2(\mu_3\text{-}O)_2]^{3+}$. Oxygenation in THF and CH_2Cl_2 followed the same procedure as above.

Resonance Raman. Resonance Raman spectra were obtained using a Princeton Instruments ST-135 back-illuminated CCD detector on a Spex 1877 CP triple monochromator with a 2400 grooves/mm holographic spectrograph grating. A laser excitation line of 413.1 nm (provided by a Coherent I90C−K Kr^+ ion laser) was chosen to enhance and probe the copper−oxygen modes. Spectral resolution was $< 2\ cm^{-1}$. Sample spectra were collected at 77 K with a liquid N_2-filled finger Dewar. The **O** species with 2 mM in Cu was formed in acetone in an NMR tube and kept frozen in liquid N_2. Isotopic substitution was achieved by oxygenation with $^{18}O_2$ (Icon, 99%).

X-ray Absorption Spectroscopy. O species suitable for X-ray absorption spectroscopy (XAS) were formed in acetone (1 mM in Cu, 5% CH_2Cl_2), and a ~200 μL of sample solution was transferred into a Lucite XAS cell with 37 μm Kapton tape windows and then frozen in liquid N_2. The X-ray absorption spectra were recorded at the Stanford Synchrotron Radiation Lightsource (SSRL) on focused 16-pole wiggler beamline 9-3 with the ring operating at 3 GeV, 80−100 mA. A Si(220) double-crystal monochromator was used for energy selection at the Cu K edge, and a Rh-coated mirror upstream of the monochromator was used for harmonic rejection, and a Rh-coated postmonochromator mirror for vertical and horizontal focusing. The samples were maintained at 10 K during data collection by using an Oxford Instruments CF1208 continuous-flow liquid-helium cryostat. Data were measured in fluorescence mode as Cu $K\alpha$ fluorescence with a Canberra (Meriden, CT) 30-element solid state Ge array detector. The internal energy calibration was performed by simultaneous measurement of the absorption of Cu foil placed between two ionization chambers filled with N_2 located after the sample. The first inflection point of the foil was assigned to 8980.3 eV. A gradual decrease in the energy of the edge region and slight changes in the EXAFS were observed upon continuous scanning at the same spot. Hence, five distinct and physically separate spots on the two XAS samples were exposed, and only two first scans at each spot were used for data analysis, for an average of four scans.

The averaged data were normalized with the program XFIT[45] by first subtracting a polynomial background absorbance that was fit to the pre-edge region and extended over the postedge with control points, followed by fitting a three-region polynomial spline of orders 2, 3, and 3 over the postedge region. The data were normalized to an edge jump of 1.0 between the background and spline curves at 9000.0 eV. Theoretical EXAFS signals $\chi(k)$ were calculated using FEFF (version 7.02)[46] and fit to the nonfiltered data by EXAFSPAK (G.N. George, SSRL). The experimental energy threshold, E_0, the point at which the photoelectron wavevector $k = 0$, was chosen as 9000.0 eV and was varied in each fit as a common value for every component in the fit. The amplitude reduction factor, S_0^2, was set to 1.0. The structural parameters that were varied during the refinements included the bond distance (R) and the bond variance (σ^2). Atom types and coordination numbers were systematically varied during the course of the analysis, but were not allowed to vary within a given fit. Data were fitted over the k range of $2-13\ Å^{-1}$. Fourier transforms of the EXAFS data and second derivatives of the normalized absorption data were calculated with EXAFSPAK.

Thermal Decomposition Kinetics. Upon the complete formation of $\mathbf{O}(CF_3SO_3)_2$ species in acetone solution of 1 mM in Cu, excess O_2 was removed by purging with N_2 for 15 min, and the $\mathbf{O}(CF_3SO_3)_2$ species was allowed to warm and decompose at specific temperatures (256−279 K), which were maintained by a thermostatic cooling bath (Kinetic systems, New York). The temperature of the sample was measured by immersing a thermocouple (Omega) into the solution. Data collection started only after the solution achieved the desired temperature, which required approximately 2−3 min. Multiwavelength (330−600 nm) component analyses of spectral data were performed with SPECFIT[47] software to obtain the decomposition rate constants. The number of significant eigenvectors obtained was two for all data sets, and a first-order kinetic (A→B) model provided good fits to these data sets.

Thermal Decomposition Product Analysis. O solution (1 mM in Cu, 5 mL acetone, $CF_3SO_3^-$) was prepared at 193 K with excess O_2 removed, and the solution was maintained at 243 K until the 392 nm band completely disappeared. Aliquots of NH_3 aqueous solution (30%) were added to the decomposed reaction product with vigorous shaking, and benzonitrile was added as an internal standard. The solution was dried over K_2CO_3 and passed through neutral activated alumina (Brockmann I, ~150 mesh, 58 Å). The column was washed with 2 mL MeOH. The combined eluent was examined by GC and GC-MS analysis.

Syntheses of Deuterated Benzyl Alcohols. The synthesis of benzyl alcohol-*d* followed the reported procedure in the literature.[18] A 1.0 g portion of benzyl alcohol was dissolved in THF, and 0.25 g of NaH (1.1 equiv) was added. After H_2 evolution ceased, the solution was filtered, and D_2O was added to the filtrate. The organic phase was separated, and the aqueous

(44) Kubas, G. J.; Monzyk, B.; Crumbliss, A. L. *Inorg. Synth.* **1979**, *19*, 90–92.

(45) Ellis, P. J.; Freeman, H. C. *J. Synchrotron Radiat.* **1995**, *2*, 190–195.

(46) Ankudinov, A. L.; Rehr, J. J. *Phys. Rev. B* **1997**, *56*, R1712–R1715.

(47) Binstead, R. A. *SPECFIT*; Spectrum Software Associates: Chapel Hill, NC, 1996.

phase was extracted with diethyl ether. The combined organic phase was dried over K_2CO_3, and the solvent was removed in vacuo to obtain benzyl alcohol-*d* (95% D by ^{1}H NMR).

Syntheses of benzyl alcohol-α-d_1 and benzyl alcohol-α,α-d_2 also followed the reported procedures in the literature.[32]

Oxidation of Exogenous Substrates. The **O** solution (1 mM in Cu, 5 mL acetone, $CF_3SO_3^-$) was prepared at 193 K with excess O_2 removed. Two equivalents of substrates (benzyl alcohol, 1-octanol or 2,4-di-*tert*-butylphenol) were added to these solutions. The reaction mixture was stirred at 243 K until the distinct **O** feature disappeared. For alcoholic substrates workup, aliquots of 30% NH_3 aqueous solution were added to the reaction mixture. Acetophenone was added as an internal GC standard. The mixture was dried over Na_2SO_4 and passed through neutral activated alumina (Brockmann I, ~150 mesh, 58 Å). The column was washed with 2 mL MeOH, and the combined eluent was examined by GC and GC-MS analyses. For phenolic substrates workup, a 10% H_2SO_4 aqueous solution (0.5 mL) was added into the cold reaction mixture before being warmed to RT. The organic phase was extracted with CH_2Cl_2, dried over Na_2SO_4, and the solvent was removed under vacuum. The residue was examined by ^{1}H NMR ($CDCl_3$, 300 MHz). The product distribution was calculated by evaluating the signals of the *tert*-butyl groups in each product: 2,4-di-*tert*-butylphenol: 1.42 ppm +1.29 ppm; 3,3′,5,5′-tetra-*tert*-butyl-2,2′-bisphenol: 1.45 ppm +1.32 ppm.

Rate Measurement of Alcohol Oxidation. Twenty equivalents of substrate ($PhCH_2OH$, $PhCH_2OD$ or $PhCD_2OH$) were added to an **O** solution (1 mM in Cu, 5 mL acetone, $CF_3SO_3^-$) with excess O_2 removed. The reaction mixture was maintained at 243 K and the decomposition of the **O** species was followed by UV−vis spectroscopy. Multiwavelength (330−600 nm) component analyses of spectral data were performed with SPECFIT[47] software to obtain the reaction rate constants. The number of significant eigenvectors obtained was two for all data sets, and a pseudo first-order kinetic (A→B) model provided good fits for these data sets.

Measurement of Intramolecular and Intermolecular Competition KIEs. Two equivalents of substrates (PhCHDOH for the intramolecular KIE, a 1:1 mixture of $PhCH_2OH$ and $PhCD_2OH$ for the intermolecular KIE) were added into the **O** solutions (1 mM in Cu, 5 mL acetone, $CF_3SO_3^-$) at 243 K. The reactions were carried out following the same procedure as described above. The organic product distribution was analyzed by GC-MS. The overall pattern of *m*/*z* 105−108 peaks in the mass spectrum of *h*- and *d*-benzaldehyde was fitted by a linear combination of individual patterns of *h*- and *d*-benzaldehyde.

Computational Details. Density functional theory (DFT) calculations were performed using a Gaussian 03 program[48] (revision C.02) on a Linux cluster. The unrestricted wave function was used for the singlet ground state of $[(TMED)_2Cu(III)_2(\mu_2\text{-}O)_2]^{2+}$. The functionals are pure functional BLYP,[49,50] hybrid functionals B3LYP[51] and BHandHLYP (as implemented in Gaussian 03) with 20% and 50% of HF exchange respectively. Basis Set 1 (BS1) uses a triple-ζ 6-311+G(d) basis set on Cu, O, and N atoms and a double-ζ 6-31G(d) basis set on C and H atoms.

The geometry optimizations were performed using the above three functionals with BS1 or 6-31G(d) basis set, followed by frequency calculations on each optimized structure with corresponding functional/basis set. Time-dependent density functional theory[52] (TD-DFT) calculations were performed using the above functionals and basis sets on the geometry optimized in vacuum by the B3LYP/6-31G(d) method. The polarized continuum model[53] (PCM) was used in the TD-DFT calculations to model the solvation environment in acetone (dielectric $\varepsilon = 20.7$) with a United Atom (UA0) radii scheme. UV−vis spectra were simulated using the SWizard[54] program with a Gaussian model and FWHM of 2500 cm^{-1}. Mulliken population analysis of molecular orbitals was calculated using the AOMix program.[55]

Acknowledgment. Funding was provided by the NIH GM50730 (T.D.P.S.), NIH DK31450 (E.I.S.), and NIH RR-01209 (K.O.H.). XAS data were measured at SSRL that is supported by the Department of Energy, Office of Basic Energy Sciences. The Structural Molecular Biology program at SSRL is funded by the National Institutes of Health, National Center for Research Resources, Biomedical Technology Program, and the Department of Energy, Office of Biological and Environmental Research. This publication was made possible by Grant 5 P41 RR001209 from the National Center for Research Resources (NCRR), a component of the National Institutes of Health (NIH). Its contents are solely the responsibility of the authors and do not necessarily represent the official view of NCRR or NIH.

Supporting Information Available: Full reference of Gaussian 03, titration of the TMED **O** species with FcCOOH, X-ray absorption spectroscopy of the **O** species with $CF_3SO_3^-$ and SbF_6^-, Eyring plot of the TMED **O** decomposition, Cartesian coordinates of the optimized D_2 conformation of the TMED **O** species, and Mulliken population analysis of selected molecular orbitals. This material is available free of charge via the Internet at http://pubs.acs.org.

(48) Frisch, M. J. et al. *Gaussian 03*, Revision C.02; Gaussian, Inc.: Wallingford, CT, 2004.
(49) Becke, A. D. *Phys. Rev. A* **1988**, *38*, 3098–3100.
(50) Lee, C. T.; Yang, W. T.; Parr, R. G. *Phys. Rev. B* **1988**, *37*, 785–789.
(51) Becke, A. D. *J. Chem. Phys.* **1993**, *98*, 5648–5652.
(52) Stratmann, R. E.; Scuseria, G. E.; Frisch, M. J. *J. Chem. Phys.* **1998**, *109*, 8218–8224.
(53) Barone, V.; Cossi, M.; Tomasi, J. *J. Comput. Chem.* **1998**, *19*, 404–417.
(54) Gorelsky, S. I. *SWizard program*; University of Ottawa: Ottawa, Canada, 2009; http://www.sg-chem.net/.
(55) Gorelsky, S. I. *AOMix: Program for Molecular Orbital Analysis*; University of Ottawa: Ottawa, Canada, 2009; http://www.sg-chem.net/.